A Highly Selective and Stable Ruthenium-Nickel Supported on Ceria Catalyst for Carbon Dioxide Methanation

Nathalie Elia, Jane Estephane, Christophe Poupin, Bilal El Khoury, Laurence Pirault-Roy, Samer Aouad, Edmond Abi-Aad

Accepted manuscript: ChemCatChem (The European Society Journal for Catalysis) (2021) **13**,**(6)** 1559-1567 https://chemistry-europe.onlinelibrary.wiley.com/doi/10.1002/cctc.202001687

A Highly Selective and Stable Ruthenium-Nickel Supported on Ceria Catalyst for Carbon Dioxide Methanation

Nathalie Elia,[a,c] Jane Estephane,*[b] Christophe Poupin,[c] Bilal El Khoury,[a] Laurence Pirault-Roy,[d] Samer Aouad,*[a] and Edmond Abi Aad,[c]

[a] Dr. N. Elia, B. El Khoury, Prof. S. Aouad,
Department of Chemistry, Faculty of Arts and Sciences University of Balamand
Kelhat, Deir El Balamand (Lebanon)
E-mail: samer.aouad@balamand.edu.lb

[b] Dr. J. Estephane
Department of Chemical Engineering Faculty of Engineering, University of Balamand
Kelhat, Deir El Balamand (Lebanon)
E-mail: jane.estephane@balamand.edu.lb

[c] Dr. N. Elia, Dr. C. Poupin, Prof. E. Abi Aad
Unité de Chimie Environnementale et Interactions sur le Vivant (UCEIV - E.A. 4492) Université du Littoral Côte d'Opale, MREI, 59140, Dunkerque (France)

[d] Prof. L. Pirault-Roy
Institut de Chimie des Milieux et des Matériaux de Poitiers (IC2MP) Université de Poitiers
UMR 7285 CNRS, 86073 Poitiers Cedex 9 (France)

Abstract: The performance of nickel, ruthenium, and nickel- ruthenium impregnated on cerium oxide catalysts was tested in the methanation of carbon dioxide reaction. The nickel and ruthenium contents were 4wt% and 0.4wt% respectively. The properties of the catalysts were studied using elementary analysis, Brunauer-Emmet- Teller specific surface area measurements, X-ray diffraction, temperature programmed reduction, temperature programmed desorption, H_2 chemisorption and transmission electron microscopy. The results showed that the addition of ruthenium improves the catalytic performance by promoting the dispersion of nickel species over the surface of the cerium oxide support. The ruthenium-nickel combination produced a stable catalyst that did not show any deactivation even after 75 hours on-stream. At high feed gas total pressures (5 and 10 bar), the catalytic conversions of CO_2 were close to the thermodynamic equilibrium values with a 100% selectivity towards CH_4 formation.

Keywords: cerium oxide • methanation • nickel • ruthenium • supported catalyst

Introduction

By general consensus, the most serious environmental problem facing humanity today is global climate change. Most atmospheric scientists are now convinced that this climate change results mainly from the anthropogenic enhancement of the greenhouse effect caused by ever-increasing levels of carbon dioxide and other “greenhouse gases”. The ambient air concentration

of CO_2 in the atmosphere has been increasing from its preindustrial times value of 280 ppm to exceed the 400 ppm during the last decade.[1] Various strategies have been proposed to reduce the carbon dioxide concentration in the atmosphere, such as the carbon capture and storage[2] or the conversion into other useful products.[3]

The synthetic production of methane via the methanation of CO_2 (Sabatier's reaction, [Equation (1)]) constitutes both an environmental (recycling of CO_2) and economical (reduction in natural gas imports) assets. The hydrogen needed for this reaction can be potentially produced by electro-catalytic or photocatalytic water splitting.[4]

$$CO_2 + 4H_2 \leftrightarrow CH_4 + 2H_2O$$
$$\Delta H_{298} = -165 \text{ kJ mol}^{-1} \qquad (1)$$

According to "Le Châtelier" principle, low temperatures will shift the equilibrium towards products formation. However, the forward reaction requires a high energy input to activate the very stable CO_2 molecule, and therefore exhibits serious kinetic limitations. In addition, at high temperatures (>450°C), CO production by the reverse water gas shift (RWGS) reaction becomes favored [Equation (2)]:[5]

$$CO_2 + H_2 \leftrightarrow CO + H_2O$$
$$\Delta H_{298} = 41.2 \text{ kJ mol}^{-1} \qquad (2)$$

Increasing the pressure can counteract the negative effect of increasing the reaction temperature. Higher pressure levels improve the methane yield of the Sabatier reaction. However, a higher process pressure has a major impact on the design of the process equipment and will drive costs. A gas feed pressure between 5 and 20 bar seems to be an ideal compromise considering both effects. Therefore, it is preferred to perform the methanation reaction at high pressures in order to make a potential industrial application economically viable.[6] This is well reported in literature, and is being applied in many current research projects such as the "Integrated High-Temperature Electrolysis and Methanation for Effective Power to Gas Conversion (HELMETH)" (up to 30 bar) and the "High Efficiency Power-to-Methane Pilot (HEPP)" (up to 10.5 bar). In addition, some companies like HZI ETOGAS are already developing and building "Power to Synthetic Natural Gas" plants in which the methanation process is carried out at higher than atmospheric pressure (3 bar).

Nickel based catalysts are the material of choice to catalyze the CO_2 methanation reaction due to their high activity and low cost.[7] However, nickel based catalysts suffer from sintering which causes unstable performances leading to deactivation. In addition, the Ni catalyst may deactivate due to the formation of di- or tri-carbonyls and stable polycarbonates which block the CO_2 adsorption sites.[8] On the other hand, the use of noble metal based catalysts proved its efficiency in the methanation reaction.[9] It was reported that, doping nickel based catalystswith noble metals, such as Ru and Rh, inhibits nickel sintering and stabilizes the catalytic performance in some reforming reactions.[10] Several literature reports discuss the benefits of combining nickel and ruthenium, creating an interaction that helps in the self-activation and stability of the catalyst.

The enhanced stability originates from the carbonyl species being important for Ru containing catalysts. [11] Moreover, it seems that the formation of bi-metallic Ni-Ru clusters improves nickel dispersion.[12] for example, bimetallic Ru-Ni systems were already reported in literature: Ni(10%)-Ru(1%)/Al_2O_3, Ni(12%)-Ru(0.5%)/Al_2O_3, Ni(30%)-Ru(3%)/$Ce_{0.9}Zr_{0.1}O_2$.[13] When it comes to catalytic supports, oxides such as Al_2O_3, TiO_2, ZrO_2, SiO_2 and CeO_2 are the most commonly used for nickel catalysts to be used in the methanation reaction. CeO_2 has excellent redox properties due to the very quick reduction of Ce^{4+} to Ce^{3+} associated with the creation of oxygen vacancies which can greatly increase redox reactions rates.[14] Moreover, the fact that an oxygen vacancy on the CeO_2 surface, is a Lewis base, it facilitates the adsorption of a CO_2 molecule and assists in its activation. Several studies reported that basic sites favor for the methanation reaction.[15]

In this work, we investigate the performance of Ru-Ni/CeO_2 catalysts, with relatively low active phase metals content (Ru 0.4 wt% and Ni 4 wt%), in the CO_2 methanation reaction. We then evaluate the performance of the bimetallic Ru-Ni/CeO_2 catalyst while varying the feed pressure between 1 and 10 bar. Finally, an aging study is carried out in order to test the stability of the catalyst and to compare its overall performance to the most recently reported methanation catalysts.

Results and Discussion

1. Catalysts Characterization

The nickel and ruthenium loadings of the different catalysts are shown in Table 1. The values are very close to the desired content, in the monometallic and bimetallic catalysts. The BET surface areas of the calcined catalysts are also listed in Table 1. Owing to the low ruthenium content (0.4 wt%), the specific surface area of the Ru/CeO_2 catalyst was similar to that of CeO_2. However, the specific surface areas of Ni/CeO_2 and Ru-Ni/CeO_2 catalysts decreased by about 25% compared to that of CeO_2. This can be explained by the pore filling during the catalyst preparation step.[16]

Table 1. Experimental metal loading from ICP analysis and specific surface areas of the calcined catalysts.

Catalyst	Ru /wt%	Ni /wt%	Specific surface area /$m^2\ g^{-1}$
CeO2	-	-	81
Ru/CeO2	0.43	-	79
Ni/CeO2	-	4.07	63
Ru-Ni/CeO2	0.37	4.43	57

The XRD patterns of the catalysts Ni/CeO_2, Ru/CeO_2 and $Ru\text{-}Ni/CeO_2$ are reported in Figure 1. The diffraction peaks of CeO2 crystallized in a fluorite phase (JCPDS 34-0394) were detected for all the catalysts.[17] The RuO2 diffraction peaks were not observed probably due to the low content of these crystals and/or its high dispersion on the CeO2 surface.[18] NiO diffraction peaks were not detected for Ni/CeO_2 and $Ru\text{-}Ni/CeO_2$, which suggests that Ni species are highly dispersed on the support.[18]]

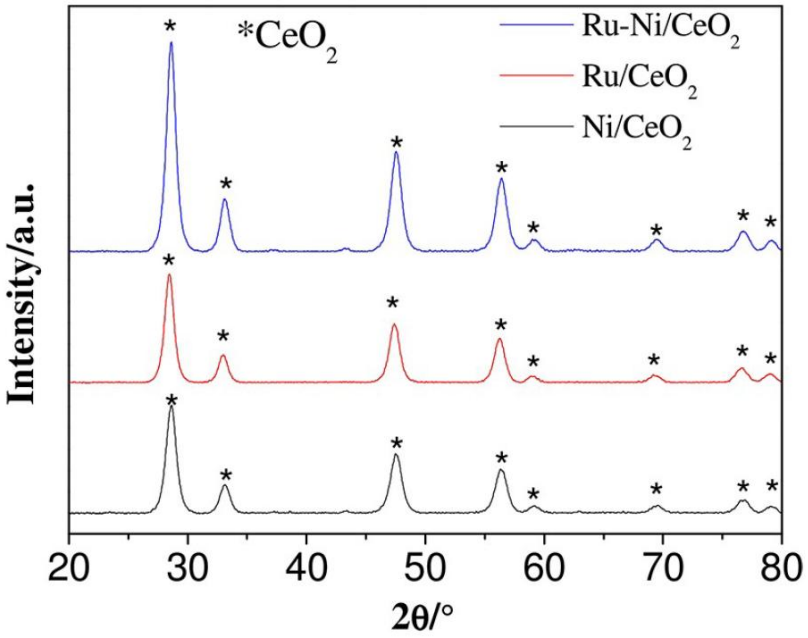

Figure 1. XRD patterns of the calcined Ru/CeO_2, Ni/CeO_2 and $Ru\text{-}Ni/CeO_2$ catalysts.

The CO_2-TPD was carried out to determine the CO_2 adsorption capacity of the catalysts in addition to the strength of the available basic sites (Figure 2). CO_2 desorption profiles, for the support CeO_2 and for all catalysts, showed only one peak at around 113°C attributed to the interaction of CO_2 with weak basic sites.[20] Therefore, chemisorption at weak basic sites corresponding to the 50–200 °C temperature range are predominant in the considered catalysts. The concentration of weak basic sites was practically similar in the support and in the monometallic and bimetallic catalysts (Figure 2), thus, all the catalysts presented the same basicity.

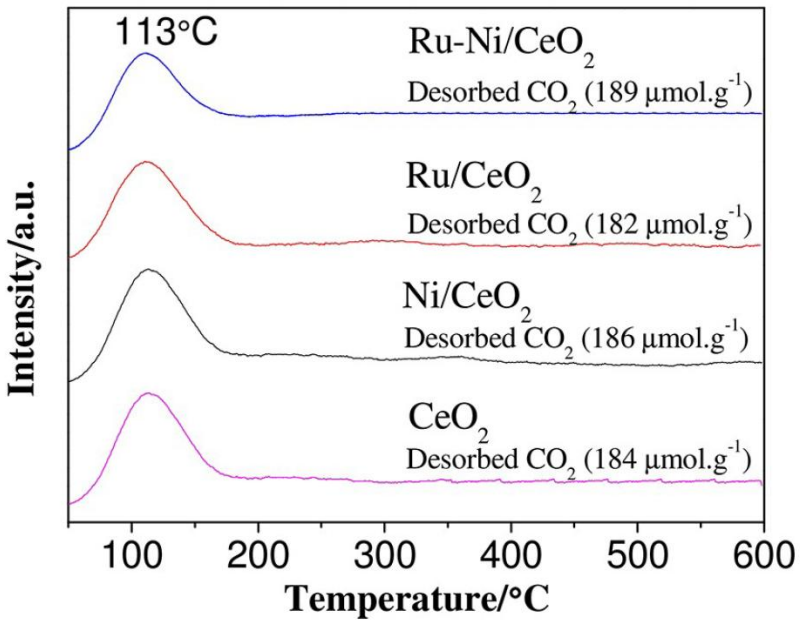

Figure 2. CO_2-TPD profiles of the CeO_2 support and calcined Ni/CeO_2, Ru/CeO_2 and $Ru\text{-}Ni/CeO_2$ catalysts.

This confirms that the CO_2 adsorption occurs mainly on the oxygen vacancies present at the surface of the CeO_2 support, while metals constituting the active phase had no significant influence on the CO_2 adsorption capacity.[21] It is worth noting that no CO emissions were detected during the desorption step indicating that the CO_2 decomposition requires the presence of the H_2 molecules in the gas feed.

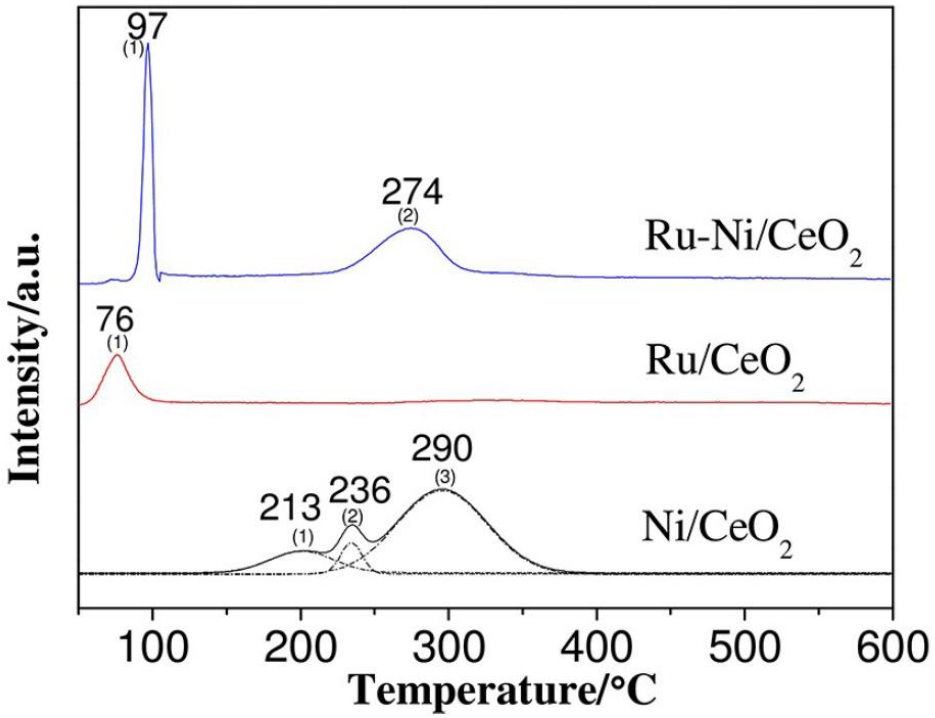

Figure 3. TPR profiles of the calcined Ni/CeO_2, Ru/CeO_2 and $Ru\text{-}Ni/CeO_2$ catalysts.

Table 2. H_2 consumption (TPR), metallic accessibility (H_2 chemisorption) and particles diameter (H_2 chemisorption and TEM) of the Ru/CeO_2, Ni/CeO_2 and $Ru\text{-}Ni/CeO_2$ catalysts.

Catalyst		Ru/CeO2	Ni/CeO2	Ru-Ni/CeO2
H_2 consumption/μmol g^{-1}	Theoretical	RuO2 : 85	NiO : 693	RuO2 : 73 NiO : 755
	Experimental	Peak1 : 314	Peak1 : 170 Peak2 : 81 Peak3 : 931	Peak1 : 420 Peak2 : 632
Metallic accessibility	H_2 uptake [μmol g^{-1}]	0.015	3.73	8.40
	Dispersion [%]	0.3	4.0	9.7
d [a] / nm		-	20.9	8.6
d [b] / nm		4.8	8.0	3.8

[a] Estimated from H_2 chemisorption. [b] Estimated from TEM micrographs.

Figure 3 shows the H_2-TPR profiles recorded for the three calcined catalysts. The Ni/CeO_2 has a TPR profile with reduction peaks in the 130–420°C temperature range. It is generally known that, large NiO particles reduce at a higher temperature than smaller ones, due to the diffusion limitation of H_2.[22] The first peak observed at 213°C can be attributed to the reduction of very small NiO particles. The second peak observed at 236 °C corresponds to the reduction of NiO particles of larger sizes. The third peak centered at 290°C is attributed to the reduction of larger NiO particles along with a part of surface ceria.[16] In fact, the experimental hydrogen consumption of these peaks (1182 μmol g^{-1}) (Table 2) is larger than the theoretical consumption corresponding to the reduction of NiO (693 μmol g^{-1}). This can be explained by a simultaneous reduction of surface cerium oxide sites along with the reduction of nickel oxides species. In fact, the reduction of surface CeO_2 into Ce_2O_3 in pure cerium oxide powders is well documented and occurs at a maximum rate in the 450-500°C temperature range.[14c] However, the presence of an active phase that reduces at lower temperatures, NiO in our case, facilitates the spillover of the H_2 molecules over the reduced Ni metal particles. The formed "H" radicals are then readily available to combine with surface oxygen atoms, removing them from the surface of the support, and creating additional oxygen vacancies.[22b,23]

The TPR profile of the Ru/CeO_2 catalyst presents one peak at 76°C. The corresponding H2 consumption is higher compared to the theoretical value (Table 2), indicating that reduction of RuO_2 to Ru0 occurs along with the reduction of surface ceria, which is promoted by the presence of metallic ruthenium.[14b] In a previous work, we showed that, in Ru/CeO_2 calcined solids,"Ru-O-Ce" oxygen bridging bonds are created between ruthenium and surface cerium. This bridging oxygen is very labile and readily reduces at low temperatures.[14c] For the $Ru\text{-}Ni/CeO_2$ catalyst, the first peak at 97°C, corresponds to the reduction of ruthenium oxide and surface ceria, since the H_2 consumption from this peak (peak 1, Table 2) is higher than the theoretical value (73 μmol g^{-1})

calculated for the reduction of RuO_2 into Ru^0. It is important to note that the three peaks attributed to the reduction of different NiO species in the Ni/CeO_2 catalyst were not observed for the $Ru\text{-}Ni/CeO_2$ catalyst.

Instead, one reduction peak centered at 274 °C is obtained. This indicates that impregnation of ruthenium on the calcined Ni/CeO_2 catalyst modified the interactions existing between the NiO particles and the ceria support. From a simple analysis of the H_2 consumption values, it is deduced that the reduction of ruthenium oxides, some nickel oxides and some surface ceria occurred simultaneously at relatively low temperatures (97 °C). The remaining NiO species presented similar interactions with the support and were uniformly reduced at 274 °C. Such results were already reported by Moreas et al. in a Pt promoted Ni/CeO_2 catalyst.[[24] It is generally accepted that small NiO particles are more readily reduced compared to larger ones. This is mainly due to a better accessibility/exposure of small particles and to H_2 diffusion limitations with respect to large particles.

Our TPR results suggest that, following the impregnation of ruthenium, NiO particles size distribution was modified, favoring the formation of additional small NiO particles. These latter are more likely present in the vicinity of ruthenium oxide species.[25] This justifies the simultaneous reduction of these metal oxides at relatively low temperatures. For all three catalysts, the reduction of the active phase was complete before 500°C (Figure 3). Therefore the pretreatment for 4 hours at 500°C under a H_2/Ar mixture before the catalytic test was sufficient to ensure the presence of only metallic Ru and Ni particles.

The H_2 chemisorption and metal dispersion results are presented in Table 2. Since the chemisorption of metallic ruthenium and nickel cannot be distinguished for the $Ru\text{-}Ni/CeO_2$ catalyst, surface metals (M_{sur}) are considered altogether for this catalyst. The metal dispersion, M_{sur}/M_{bulk}, is estimated from H_{ad}/M_{bulk} ratio assuming a chemisorption stoichiometry H/M = 1 for all the catalysts.[26] The chemisorbed H_2 amount for the Ru- Ni/CeO_2 catalyst (8.4 µmol g^{-1}) was much higher than the summation of H_2 uptakes (3.745 µmol g^{-1}) obtained for the individual monometallic catalysts. The dispersion of the active phase in the $Ru\text{-}Ni/CeO_2$ catalyst (9.7%) was ~2.5 times greater than the one observed for the Ni/CeO_2 catalyst (4%). Similar observations were reported by Crisafulli et al. in the case of a $Ru\text{-}Ni/SiO_2$ catalyst.[27] This correlates well with our TPR results that suggested a different distribution of Ni species in the presence of ruthenium.

Figure 4 displays representative TEM images and particle size distributions for the monometallic and bimetallic catalysts, respectively. In the case of the Ni/CeO_2 catalyst, a heterogeneous distribution of nickel particles and the average diameter is equal to 8.3 nm. The metallic active phase is more homogeneously dispersed on the support in the $Ru\text{-}Ni/CeO_2$ catalyst, with a smaller average diameter of 3.8 nm. Table 2 shows that the particle diameters determined from H_2 chemisorption are larger than those determined from TEM images. This difference can be explained by the presence of a few particles of nickel of much larger size that would not be observed by TEM. In fact, it is difficult to visualize the nickel particles, due to the lack of contrast between nickel and ceria. However, both techniques revealed a similar trend in which the bimetallic catalyst presents smaller metal particle sizes (by a factor of 2.2 to 2.5). This confirms the previous suggestion that the addition of Ru favored the dispersion of nickel species. This has facilitated the reduction of nickel oxide species, and led to the formation of a well dispersed active

phase that is will be potentially more active in the considered reaction.

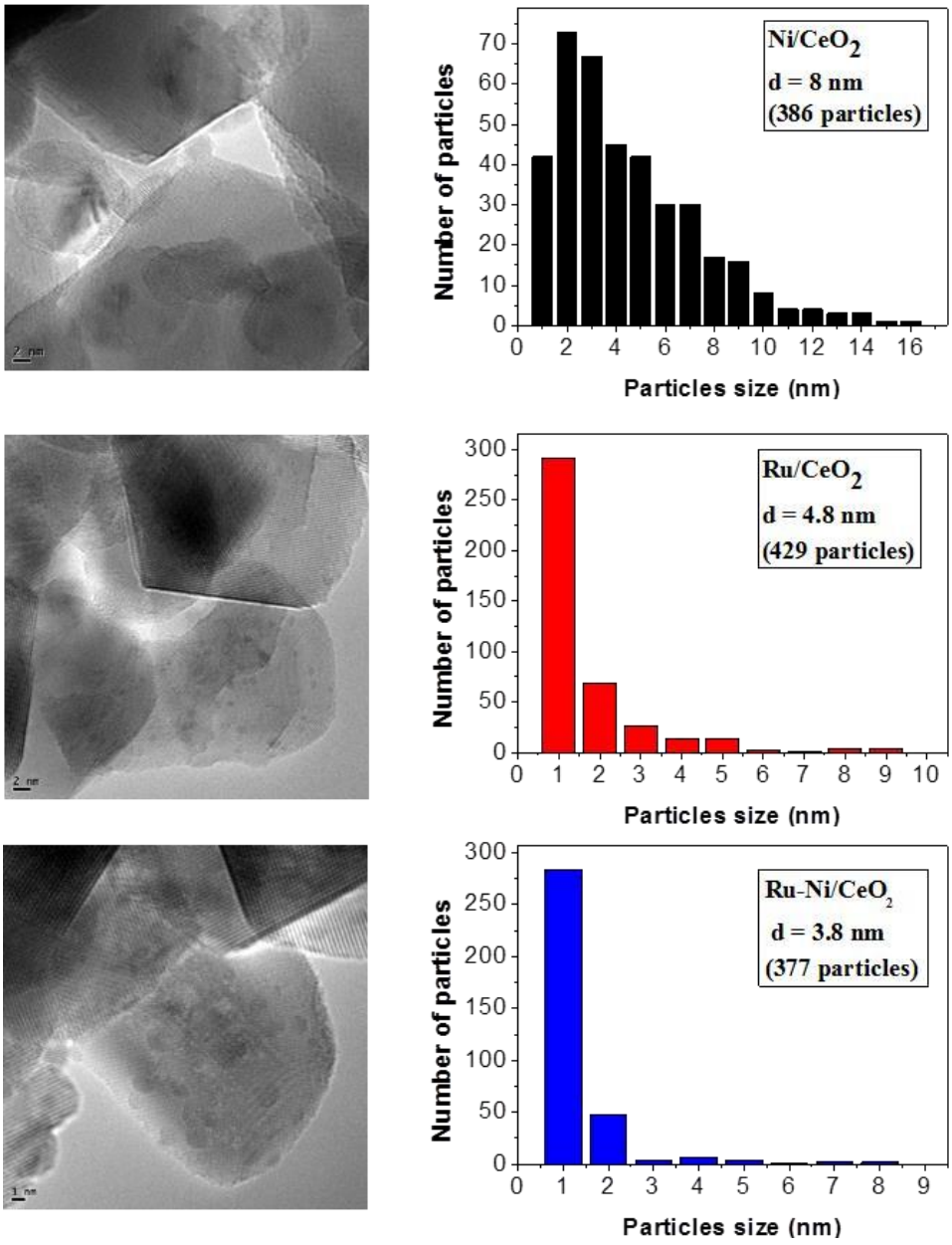

Figure 4. TEM micrographs and particle size distributions for the a) Ni/CeO2, b) Ru/CeO2 and c) Ru-Ni/CeO2 catalysts.

Catalytic activity

The catalytic performances of the different catalysts in the CO_2 methanation reaction are presented in figure 5. Figure 5 (a) shows that, whatever the catalyst, the CO_2 conversion increased with increasing temperature. The Ru-Ni/CeO2 catalyst gave the best conversions amounting to 44% at 300°C and 70% at 350°C. The Ru-Ni/CeO2 catalyst was also very selective towards CH_4 production with selectivity values close to 100% (figure 5 (b)). The monometallic catalyst Ru/CeO2 gave the lowest CO_2 conversion (14% at 350°C). This is probably due to the low ruthenium content. The bimetallic synergestic effect in the Ru- Ni/CeO2 catalyst is backed with previous results[28] where the addition of 0.5 wt% ruthenium to Ni(10%)/CeO2 didn't improve the catalytic conversion of CO_2. In the same work, we proved that starting with Ni(5%)/CeO2 and

promoting it with 0.5 wt% Ru yielded better results compared to the increase of Ni loading from 5 wt% to 10 wt%.

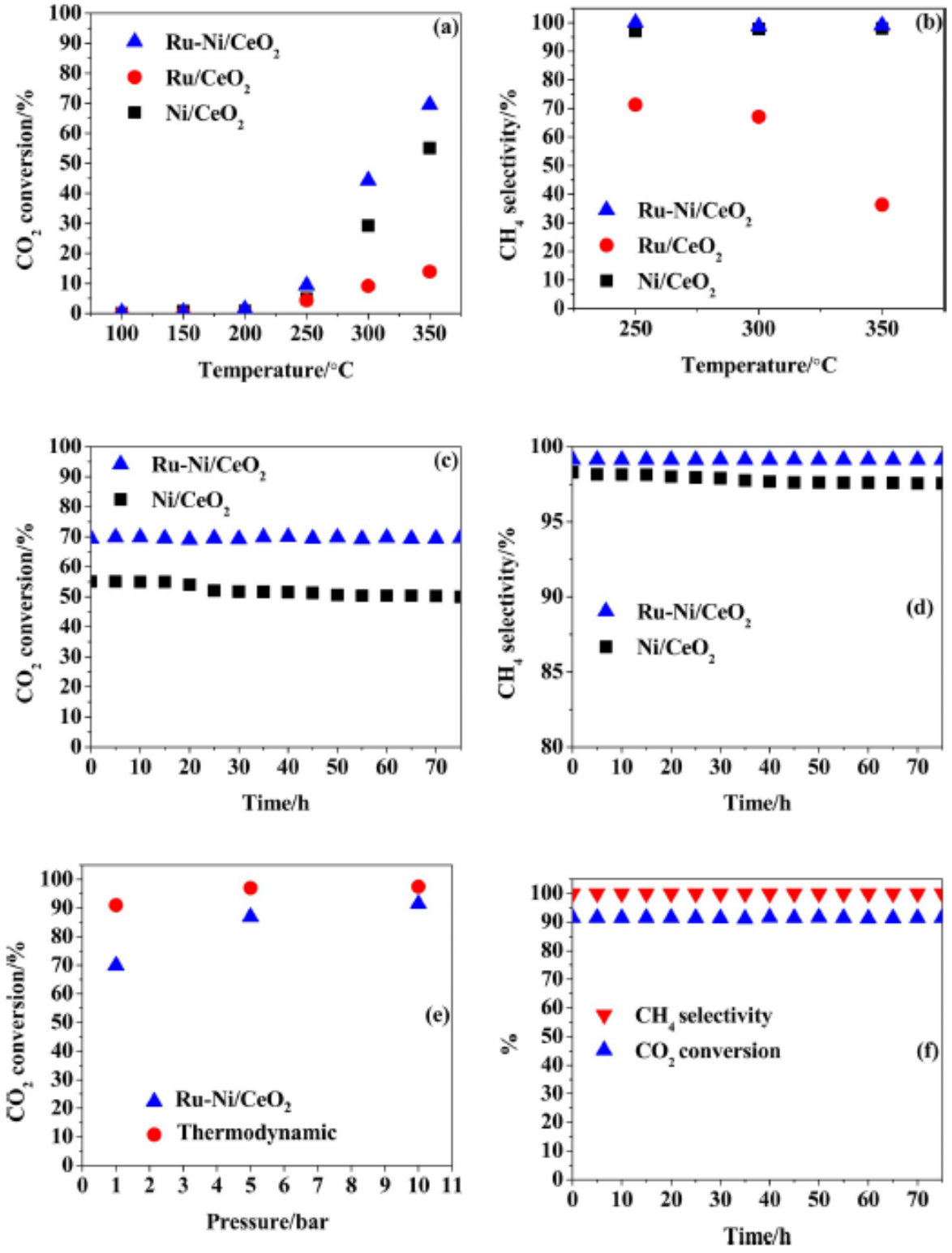

Figure 5. (a) CO2 conversion, and (b) CH4 selectivity over Ru/CeO2, Ni/CeO2 and Ru-Ni/CeO2 catalysts (P= 1bar, H2/CO2 = 4, and GHSV = 40000 mL g^{-1} h^{-1}); (c) Long-term CO2 conversion, and (d) long term CH4 selectivity test over Ni/CeO2 and Ru-Ni/CeO2 catalysts at 350°C and 1 bar (H2/CO2 = 4, and GHSV = 40000 mL g^{-1} h^{-1}); (e) CO2 conversion as a function of pressure over Ru-Ni/CeO2 catalyst and thermodynamic equilibrium at 350°C; (f) Long-term stability test over

Ru- Ni/CeO_2 catalysts at 350°C and 10 bar (H_2/CO_2 = 4, and GHSV = 40000 mL g^{-1} h^{-1}).

The TPR, hydrogen chemisorption and TEM analyses showed that in the Ru-Ni/CeO_2 catalyst, the metallic active phase is better dispersed. The presence of Ru enhanced the dispersion of metallic Ni particles, which yielded more Ni active sites.[13c,29] These latter, can promote the dissociative adsorption of CO_2 while Ru active sites promote the H_2 "spillover" which provides the "H" radicals required for the methanation reaction.[30] Several authors have demonstrated that two active sites are required for the CO_2 methanation: reduced metal species (M^0) for the dissociation and transfer of H_2 and Metal-CeO_2 in intimate contact where the CO_2 dissociation takes place and thus, an optimal amount of both sites is required to maximize the CO_2 conversion into methane.[31]

It has already been demonstrated that oxygen vacancies are generated during the reduction of CeO_2.[22a] In fact, our CeO_2 support presents crucial weak basic sites (Figure 2) that readily adsorb the CO_2 molecules and favor the methanation reaction. Tada *et al.* compared different Ni based catalysts in the CO_2 methanation reaction. They concluded that the Ni/CeO_2 catalyst is more active and produces high CO_2 conversion due to the coverage of CeO_2 surface with CO_2-derived species and the partial reduction of CeO_2 surface.[32a] From the work of Pan *et al.*, one can suggest that CO_2 adsorbs preferentially on surface oxygen sites adjacent to Ce(III) compared with those adjacent to Ce(IV) or surface hydroxyl sites. [8c] This observation was made in most of the studies considering a CeO_2 supported catalysts or a mixed oxide support containing CeO_2.[31b] In the literature, Different types of adsorbed species were reported to form on Ni/CeO_2 catalysts in the presence of CO_2 in the gas phase. Hydrogen carbonate species, bidentate carbonate species, monodentate carbonate species and bridged carbonate species were all observed in the study of Lee *et al*.[21b] However, the authors proved that bridged carbonate species were adsorbed on oxygen vacancies present in CeO_2 support and not on reduced Ni particles. When H_2 is present along with CO_2 in the gaseous mixture, formate species are observed, and it is believed that it originates from hydrogen carbonate species and monodentate carbonate species.[21b,31b] Most of the literature suggests that formate species are the major intermediates during the methanation reaction over CeO_2 supported catalysts and that Ce^{3+} sites with oxygen vacancies are active sites for their formation and further hydrogenation. In this study, we believe that CO_2 molecules are adsorbed and activated on oxygen vacancies near Ce^{3+} sites to form different CO_2-derived adsorbed species depending on the temperature. These latter are hydrogenated into formate species by reaction with hydrogen radicals originating from the dissociation of H_2 molecules on reduced Ru/Ni active sites. The presence of hydrogen also favors the regeneration of Ce^{3+} sites that can further adsorb new CO_2 molecules. It is to note that at high temperatures (> 300°C), CO_2 can directly dissociate into CO on reduced metallic Ru/Ni particles, and CO can be then effectively hydrogenated until the formation of methane gas.[15a,32c] Table 3 contains compiled data related to some published articles, that reported CO_2 methanation in the presence of different types of catalysts.

Table 3. CO_2 conversion, CH_4 selectivity, CH_4 yield and GHSV obtained during the CO_2 methanation reaction in the presence of different catalysts reported in the literature (P=1 bar, H_2/CO_2 = 4).

Catalyst	T/ °C	CO_2 conversion/ %	CH_4 selectivity/ %	CH_4 yield/ %	Gas hourly space velocity/ mL g^{-1} h^{-1}	Publi-cation year	Ref.
Ru(0.4%)-Ni(4%)/CeO_2	350	70	99.2	69.4	40000	-	This work
Ni(15%)/RHA-Al_2O_3	500	63	90	56.7	30000	2003	[33a]
Haldor Topsøe PK-7R	350	60	-	-	-	2010	[33b]
Ru(1%)-Ni(10%)/Al_2O_3	350	68	100	68	54000	2014	[13a]
Ni(59%)/HT	350	74	-	-	1100	2016	[33c]
Ru(0.5%)-Ni(12%)/Al_2O_3	350	55	98.8	54.3	40000	2017	[13b]
Ni(10%)/CeO_2-ZrO_2	350	52	98.9	51.4	20000	2017	[33d]
Ni(39%)/Sm_2O_3	350	72	98.5	70.9	60000	2019	[33e]
Ni(10%)/Pr_2O_3-CeO_2	350	54.5	100	54.5	25000	2020	[33f]

Our catalyst is listed in first row of the table for the sake of comparison. With a CO_2 conversion of 70% and a CH_4 selectivity of 99%, the catalyst reported in this study is more efficient than most of the catalysts listed in the table. It is superior to the Ni(20-25%)/Al_2O_3 "*Haldor Topsøe PK-7R*" commercial catalyst compared at the same temperature of 350°C.[33b] A simple comparison to the listed results reveals that the 4 wt% Ni active phase content in our catalyst is much lower than the loading reported in literature that range from 10 wt% and up to 59 wt%. In addition the ruthenium content of 0.4 wt% is lower than those reported in literature.[33] The catalyst Ni(59%)/HT that had a CO_2 conversion of 74% at 350°C, was subjected to a GHSV (1100 mL g^{-1} h^{-1}) that is 36 times lower than the one used in this study (40000 mL g^{-1} h^{-1}).[33c] Therefore, the relatively higher CO_2 conversion is due to a 15 times larger Ni content and to a longer contact time of the reactant feed gas with the catalyst allowing more time for the reaction. On the other hand, the Ni(39%)/Sm_2O_3 converted 72% of the CO_2 at 350°C under a GHSV that is 1.5 times larger than the one used in this study. However, this catalyst had 10 times more Ni than the catalyst used in this study and also showed a considerable deactivation after just 10 hours on stream (CO_2 conversion dropped from 72% to ~ 60%).[33e] This brief overview served to benchmark the performance of the Ru-Ni/CeO_2 catalyst with respect to studies reported in the literature. Taking into consideration different important parameters, such as metal loading and contact time,

it appears that the present catalyst is highly active in the CO_2 methanation reaction.

The thermodynamics of the Sabatier reaction dictate that a higher feed gas pressure favors products formation. Therefore, the catalytic performance of the Ru-Ni/CeO_2 catalyst was evaluated under different pressures ranging from 1 to 10 bar (Figure 5 (e)). At 350°C, the CO_2 conversion increased from 70% at 1 bar to 87 % at 5 bar and 91 % at 10 bar. The CH_4 selectivity was 99.2% at 1 bar and reached 100% at 5 and 10 bar. It is worth noting that the gap between experimental conversions and thermodynamic equilibrium values narrowed with increasing pressure. Few studies considered the methanation of carbon dioxide at high pressure. However, Ocampo et al. studied the effect of pressure over Ni(5wt%)/$Ce_{0.72}Zr_{0.28}O_2$ catalyst.[35] They found that higher pressures led to an improvement in methane yield at 350°C. At 3 and 5 bar, CH_4 yield reached 77% and 82% respectively. A further raise in pressure to 7 bar did not allow any further improvement in CH_4 yield. Thus, the Ru-Ni/CeO_2 catalyst prepared in this study is superior to the catalyst reported in [35] for the CO_2 methanation. In addition, the Ru-Ni/CeO_2 catalyst was also perfectly stable, with no loss of actvity, over a 75 hours period under 10 bar feed gas pressure (Figure 5 (f)). This performance makes the catalyst suitable for industrial application since the industrial equipment used for methanation often operate at high pressures.

Conclusion

The presented results show that a Ru-Ni/CeO_2 catalyst with a relatively low active phase loading (Ru : 0.4 wt% and Ni 4 wt%) is active in the methanation of CO_2. The CO_2 conversion increases with temperature and equals 70% at 350°C. The Ru- Ni/CeO_2 catalyst showed a perfectly stable performance up tp 75 hours on stream. It also exhibited excellent catalytic performance at higher than atmospheric feed gas pressures, with a CO_2 conversion of 91% at 350°C and 10 bar. The stability was also kept unaltered for 75 hours on stream at 10 bar. Whatever the test conditions and duration, CH_4 selectivity was always greater than 99%. The Ru-Ni/CeO_2 catalyst outperformed the monometallic catalysts both in activity and stability in the CO_2 methanation reaction. The catalytic performance was more than additive which indicated a synergestic effect between ruthenium and nickel species. Characterization techniques revealed that the addition of ruthenium favors an enhanced dispersion of nickel species. These latter, together with the well dispersed ruthenium species, have excellent redox properties allowing it to reduce at low temperatures. This also promotes the reduction of surface ceria leading to the creation of more oxygen vacancies. The CO_2 molecule is adsorbed on oxygen vacancies near Ce^{3+} sites and forms CO_2-derived adsorbed species (monodentate carbonates, bidentate carbonates, bridged carbonates, and hydrogen carbonates). The H_2 molecule splits on the well dispersed Ni or Ru-Ni nanoparticles and hydrogen react with the adsorbed CO_2- derived species to form formate species. The catalyst surface is now primed for the formation of new bonds and the production of CH_4 and H_2O. The promotion with Ru played an important triple role a) favoring the creation of more oxygen vacancies for CO_2 adsorption; b)

enhancing the dispersion of Ni particles for a better interaction with reactants molecules; c) inhibiting the sintering of Ni particles and therefore the deactivation of the catalyst. Finally, the Ru-Ni/CeO_2 catalyst, that is prepared using a simple impregnation method is more efficient than many catalysts reported in the literature. This indicates that it is promising for practical applications in the methanation reaction.

Experimental Section

Catalysts preparation

CeO_2 was prepared as reported in by precipitation of cerium (III) nitrate hexahydrated solution $Ce(NO_3)_3.6H_2O$ with a solution of NaOH.[14b] The solid was filtered, washed, dried at 100°C and then calcined at 500°C for 4 hours. The monometallic catalysts Ni/CeO_2 and Ru/CeO_2 were prepared via incipient wetness impregnation of an aqueous solution of the corresponding precursors $Ni(NO_3)_2.6H_2O$ and $Ru(NO)(NO_3)_3$. After impregnation the samples were dried at 60°C for 12 hours and then calcined at 500°C for 4 hours in air. The bimetallic catalyst Ru-Ni/CeO_2 was prepared by successive impregnation method. The calcined support was first impregnated with $Ni(NO_3)_2.6H_2O$ solution, dried at 60°C for 12 hours, calcined at 500°C for 4 hours, and afterwards, was impregnated with $Ru(NO)(NO_3)_3$ solution. The resulting solid was dried at 60°C for 12 hours and calcined at 500°C for 4 hours.

Catalysts characterizations

Elemental analysis using inductively coupled plasma atomic emission spectroscopy (ICP-AES) technique, performed on a Perkin Elmer Optima 2000 DV apparatus, was used to determine the content of different metals present in the catalysts.

x- ray diffraction (XRD) experiments were carried out on a Bruker D8 Advance diffractometer using Cu-Kα radiation (λ = 1.5405 nm). The diffraction intensities were measured over an angular range of 20°< 2θ < 80° for all the samples with a step size of 2θ = 0.02°.

The Brunauer–Emmett–Teller (BET) surface area of the catalysts was determined from the complete nitrogen adsorption isotherms at −196°C using an ASAP 2020 Micromeritics apparatus.

Basic properties of the catalysts were studied by CO_2-temperature programmed desorption (CO_2-TPD) using an Autochem 2920 Micromeritics apparatus. 50 mg of calcined catalysts were pretreated under Helium flow (30 mL min^{-1}) at 500°C for 1 hour. The catalysts were then cooled to 50°C and then exposed to a flow of 10% CO_2/He (30 mL min^{-1}) for 1 hour. The samples were then purged with Helium (30 ml min^{-1}) for 0.5 hour and the temperature was finally raised to 500°C at a rate of 10°C min^{-1} to desorb the CO_2.

Temperature-programmed reduction (TPR) experiments were performed using an Autochem 2920 Micromeritics apparatus. 50 mg of calcined catalysts were placed on quartz wool in a U-

shaped quartz sample tube and heated from room temperature to 500°C at a rate of 10°C min^{-1} under a gaseous flow (30 mL min^{-1}) of 5% H_2 diluted in Ar. The H_2 consumption was measured with a thermal conductivity detector.

Hydrogen chemisorption was carried out by pulses at −85°C to avoid the H_2 adsorption over CeO_2. Before pulse chemisorption, the catalyst was reduced at 500°C under a flow (30 mL min^{-1}) of pure H_2 for 1 hour and then the sample was purged by passing a flow of 30 mL min^{-1} of argon at 500°C for 1 hour. The catalyst was cooled in flowing argon. The hydrogen pulse chemisorption study was done at −85°C using pure H_2. H_2 pulses were injected every 3 minutes until the area of successive hydrogen peaks were identical.

Transmission Electron Microscopy (TEM) analyses were performed on a JEOL 2100 UHR microscope. The powdered samples were dispersed in ethanol and the resulting suspensions deposited on a copper grid coated with a porous carbon film. By exploitation of the images with the ImageJ software, mean surface diameters ($d = \Sigma(nidi^3)/\Sigma(nidi^2)$) were determined by measuring at least 300 particles for each analysed sample.

Catalytic Tests

The catalytic activity was measured at different pressures using a continuous fixed-bed reactor (Microactivity, PID Eng and Tech). 150 mg of catalyst diluted with SiC to achieve a catalytic bed volume of 1 cm^3 was placed in the reactor. Prior to the reaction, the calcined samples were reduced at 500°C for 4 h under H_2/Ar (50 %) flowing at a rate of 50 mL min^{-1} with a heating rate of 5°C min^{-1}. After cooling, the reactants were introduced (CO_2: 10 vol.%, H_2: 40 vol.%, Ar: 50 vol.%) with a total flow rate of 100 mL min^{-1} (GHSV = 40000 mL g^{-1} h^{-1}). The reaction temperature was increased (5°C min^{-1}) from 100°C up to 350°C and kept for 30 minutes at each 50°C temperature interval for product gases analyses. A Varian multichannel Microgas chromatography was used for gaseous mixture analysis. The reactants (CO_2 and H_2) and main products (CH_4 and CO) where separated in a module equipped with CP- COX column and a micro-TCD.

CO_2 conversion (X_{CO_2}) and selectivity to methane (S_{CH_4}) are defined as:

$$X_{CO_2} = \frac{n\,CO_2(in) - nCO_2(out)}{n\,CO_2(in)}\,X\,100$$

$$S_{CH_4} = \frac{n\,CH_4}{n\,CO_2(in) - nCO_2(out)}\,X\,100$$

Acknowledgements

The authors would like to thank the Lebanese Council for Scientific Research (CNRS-L) through its Grant Research Program (GRP2014/05-06-14) and the “Université du Littoral — Côte d’Opale, France” for financial support.

References

[1] N. Podrojková, V. Sans, A. Oriňak, R. Oriňaková, ChemCatChem **2019**, 12, 1802-1825.

[2] a) Y. Zhang, T. Zhou, B. Louis, F. Yu, J. Dan, Q. Wang, Catalysts **2017,** 7, 105; b) D.E. Allen, B.R. Strazisar, Y. Soong, S.W. Hedges, Fuel Process. Technol. **2005,** 86, 1569-1580.

[3] a) K. Ghaib, K. Nitz, F.Z. Ben-Fares, ChemBioEng **2016**, 3, 266-275; b) S. Remiro-Buenamañana, H. García, ChemCatChem **2018**, 11, 342-356.

[4] a) E. Giglio, F.A. Deorsola, M. Gruber, S.R. Harth, E.A. Morosanu, D. Trimis, S. Bensaid, R. Pirone, Ind. Eng. Chem. Res. **2018**, 57, 4007-4018; b) F. Pellegrino, F. Sordello, M. Minella, C. Minero, V. Maurino, Catalysts **2019**, 9, 32.

[5] J. Gao, Q. Liu, F. Gu, B. Liu, Z. Zhong, F. Su, RSC Adv. **2015**, 5, 22759-22776.

[6] M. Gruber, P. Weinbrecht, L. Biffar, S. Harth, D. Trimis, J. Brabandt, O. Posdziech, R. Blumentritt, Fuel Process. Technol. **2018**, 181, 61-74;

[7] a) N. Bette, J. Thielemann, M. Schreiner, F. Mertens, ChemCatChem **2016**, 8, 2903-2906; b) Y. Wu, J. Lin, Y. Xu, G. Ma, J. Wang, M. Ding, ChemCatChem **2020**, 12, 3553-3559.

[8] a) M. Agnelli, H.M. Swaan, C. Marquez-Alvarez, G.A. Martin, C. Mirodatos, J. Catal. **1998**, 175, 117-128 ; b) M.A.A. Aziz, A.A. Jalil, S.Triwahyono, S.M. Sidik, *Appl. Catal, A* **2014**, *486*, 115-122; c) Q. Pan, J. Peng, S. Wang, S. Wang, *Catal. Sci. Technol.* **2014**, *4*, 502-509.

[9] a) S. Tada, O.J. Ochieng, R. Kikuchi, T. Haneda, H. Kameyama, *Int. J. Hydrogen Energy* **2014**, *39*, 10090-10100; b) R. Thalinger, T. Götsch, C. Zhuo, W. Hetaba, W. Wallisch, M. Stöger-Pollach. D. Schmidmair, B. Klötzer, S. Penner, *ChemCatChem* **2016**, *8*, 2057-2067.

[10] Y. Guo, L. Zhou, H. Kameyama, *Int. J. Hydrogen Energy* **2011**, *36*, 5321-5333; b) A. Al-Fatesh, S.K. Singh, G.S. Kanade, H. Atia, A.H. Fakeeha, A.A. Ibrahim, A.M. El-Toni, N.K. Labhasetwar, *Int. J. Hydrogen Energy* **2018**, *43*, 12069-12080.

[11] a) S. Akamaru, T. Shimazaki, M. Kubo, T. Abe, *Appl. Catal. A* **2014**, *470*, 405-411; b) Z. Gao, L. Cui, H. Ma, *Int. J. Hydrogen Energy* **2016**, *41*, 5484-5493; c) J. Polanski, T. Siudyga, P. Bartczak, M. Kapkowski, W. Ambrozkiewicz, A. Nobis, R. Sitko, J. Klimontko, J. Szade, J. Lelątko, *Appl. Catal. B Environ.* **2017**, *206*, 16-23.

[12] X. Shang, D. Deng, X. Wang, W. Xuan, X. Zou, W. Ding, X. Lu*, Int. J. Hydrogen Energy* **2018**, *43*, 7179-7189.

[13] a) W. Zhen, B. Li, G. Lu, J. Ma, *RSC Adv.* **2014**, *4*, 16472-16479 ; b) K. Stangeland, D. Kalai, H. Li, Z. Yu, *Energy Procedia* **2017**, *105,* 2016- 2021; c) X. Shang, D. Deng, X. Wang, W. Xuam, X. Zou, W. Ding, X. Lu, *Int. J. Hydrogen Energy* **2018**, *43*, 7179-7189.

[14] a) S. Aouad, E. Saab, A. Aboukaïs, *Kinet. Catal.* **2007**, *48*, 893-898; b) S. Aouad, E. Saab, E. Abi Aad, A. Aboukaïs, *Catal. Today* **2007**, *119*, 273-277; c) S. Aouad, E. Abi-Aad, A. Aboukaïs, *Appl. Catal. B Environ.* **2009**, *88*, 249-256.

[15] a) P.A.U. Aldana, F. Ocampo, K. Kobl, B. Louis, F. Thibault-Starzyk, M. Daturi, P. Bazin, S. Thomas, A.C. Roger, *Catal. Today* **2013**, *215*, 201- 207; b) Q. Pan, J. Peng, T. Sun, S. Wang, S. Wang, *Catal. Commun.* **2013**, *45*, 74-78; c) X. Guo, A. Traitangwong, M. Hu, C. Zuo, V. Meeyoo, Z. Peng, C. Li, *Energy & Fuels* **2018**, *32*, 3681-3689.

[16] a) T.A. Le, M.S. Kim, S.H. Lee, T.W. Kim, E.D. Park, *Catal. Today* **2017**, *293-294*, 89-96; b) R. Mahfouz, J. Estephane, C. Gennequin, L. Tidahy, S. Aouad, E. Abi-Aad, *J. Env. Chem. Eng.* **2020**, 104662.

[17] A. Aboukaïs, M. Skaf, S. Hany, R. Cousin, S. Aouad, M. Labaki, E. Abi- Aad, *Mater. Chem. Phys.* **2016**, *177*, 570-576.

[18] S. Tada, R. Kikuchi, K. Wada, K. Osada, K. Akiyama, S. Satokawa, Y. Kawashima, *J. Power Sources* **2014**, *264*, 59-66.

[19] W. Kang, A. Varma, *Appl. Catal. B Environ.* **2018**, *220*, 409-416.

[20] L. Bian, L. Zhang, R. Xia, Z. Li, *J. Nat. Gas Sci. Eng.* **2015**, *27*, 1189-1194.

[21] a) M. Mihet, M.D. Lazar, *Catal. Today* **2018**, *306*, 294-299; b) S.M. Lee, Y.H. Lee, D.H. Moon, J.Y. Ahn, D.D. Nguyen, S.W. Chang, S.S. Kim, *Ind. Eng. Chem. Res.* **2019**, 58, 20, 8656-8662.

[22] a) X. Liao, Y. Zhang, M. Hill, X. Xia, Y. Zhao, Z. Jiang, *Appl. Catal. A Gen.* **2014**, *488*, 256-264; b) R.K. Singha, A. Shukla, A. Yadav, L.N. Sivakumar Konathala, R. Bal, *Appl. Catal. B Environ*. **2017**, *202*, 473- 488.

[23] P.V.R. Rao, V.P. Kumar, G.S. Rao, K.V.R. Chary, Catal. Sci. Technol. 2012, 2, 1665-1673.

[24] T.S. Moraes, R.C.R. Neto, M.C. Ribiero, L.V. Mattos, M. Kourtelesis, S. Ladas, X. Verkiyos, F.B. Noronha, Appl. Catal. B Environ. 2016, 181, 754-768.

[25] L.J. Li, W.J. Yi, T.W. Liu, C. Huang, Z.S. Chao, RSC Adv. 2017, 7, 32027-32037.

[26] J.C.S. Wu, H.C. Chou, Chem. Eng. J. 2009, 148, 539-545.

[27] C. Crisafulli, S. Scire, R. Maggiore, S. Minico, S. Galvagno, Catal. Letters 1999, 59, 21-26.

[28] N. Elia, PhD thesis, Université du Littoral – Côte d'Opale (FR), 2019.

[29] F. Ocampo, B. Louis, L. Kiwi-Minsker, A.C. Roger, Appl. Catal. A Gen. 2011, 392, 36-44.

[30] Y. Liu, W. Sheng, Y. Zhang, RSC Adv. 2018, 8, 2123–2131.

[31] a) J.H. Kwak, L. Kovarik, J. Szanyi, ACS Catal. 2013, 3, 2094-2100; b) M.A.A. Aziz, A.A. Jalil, S. Triwahyono, A. Ahmad, Green Chem. 2015, 17, 2647-2663.

[32] a) S. Tada, T. Shimizu, H. Kameyama, T. Haneda, R. Kikuchi, Int. J. Hydrogen Energy, 2012, 37, 5527-5531; b) F. Wang, M. Wei, D.G. Evans, X. Duan, J. Mater. Chem. A 2016, 4, 5773-5783; c) G. Zhou, H. Liu, K. Cui, A. Jia, G. Hu, Z. Jiao, Y. Liu, X. Zhang, Appl. Surf. Sci. 2016, 383, 248-252

[33] a) F.W. Chang, M.S. Kuo, M.T. Tsay, M.C. Hsieh, *Appl. Catal. A Gen.* **2003**, *247*, 309-320; b) S.K. Hoekman, A. Broch, C. Robbins, R. Purcell, *Int. J. Greenh. Gas. Con.* **2010**, *4*, 44-50; c) N. Bette, J. Thielemann, M. Schreiner, F. Mertens, *ChemCatChem* **2016**, *8*, 2903-2906; d) J. Ashok, M.L. Ang, S. Kawi, *Catal. Today* **2017**, *281*, 304-311; e) J. Ilsemann, A. Sonström, T.M. Gesing, R. Anwander, M. Bäumer, *Chemcatchem* **2019**, *11*, 1732-1741; f) G.I. Siakavelas, N.D. Charisiou, S. Al Khoori, A.A. Al Khoori, V. Sebastian, S.J. Hinder, M.A. Baker, I.V. Yentekakis, K. Polychronopoulou, M.A. Goula, *Appl. Catal. B Environ.* **2020**, 119562, https://doi.org/10.1016/j.apcatb.2020.119562.

[34] a) G. Li, L. Hu, J.M. Hill, *Appl. Catal. A Gen.* **2006**, *301*, 16-24 ; b) L. Zhang, C. Xu, P. Champagne, *Fuel* **2012**, *96*, 541-545.

[35] F. Ocampo, B. Louis, A. Kiennemann, A.C. Roger, *IOP Conf. Ser. Mater. Sci. Eng.* **2011**, *19*, 012007.